Atmospheric Research 213 (2018) 211–223

Contents lists available at ScienceDirect

Atmospheric Research

journal homepage: www.elsevier.com/locate/atmosres

The influence of volcanic eruptions on weather regimes over the North Atlantic simulated by ECHAM5/MPI-OM ensemble runs from 800 to 2000 CE

H. Guðlaugsdóttir[a,b,*], H.C. Steen-Larsen[c], J. Sjolte[d], V. Masson-Delmotte[e], M. Werner[f], Á.E. Sveinbjörnsdóttir[a,b]

[a] Institute of Earth Sciences, University of Iceland, Iceland
[b] Nordic Volcanological Centre (NordVulk), Institute of Earth Sciences, University of Iceland, Iceland
[c] Geophysical Institute, University of Bergen and Bjerknes Centre for Climate Research, Bergen, Norway
[d] Department of Geology, Lund University, Sweden
[e] LSCE (UMR 8212 CEA-CNRS-UVSQ), Université Paris Saclay, Institut Pierre Simon Laplace, France
[f] Alfred Wegener Institute (AWI), Helmholtz Centre for Polar and Marine Research, Bremerhaven, Germany

A B S T R A C T

The volcanic fingerprint on the winter North Atlantic atmospheric circulation and climate is analyzed in six ensemble runs of ECHAM5/MPI-OM covering 800–2000 CE, both for equatorial and Northern Hemisphere (NH) eruptions. Large volcanic eruptions influence climate on both annual and decadal time scales due to dynamic interactions of different climate components in the Earth's system. It is well known that the North Atlantic Oscillation (NAO) tends to shift towards its positive phase during winter in the first 1–2 years after large tropical volcanic eruptions, causing warming over Europe, but other North Atlantic weather regimes have received less attention. Here we investigate the four dominant weather regimes in the North Atlantic: The negative and positive phase of NAO as well as the Atlantic Ridge, Scandinavian blocking. The volcanic fingerprint is detected as a change in the frequency of occurrence and anomalies in the wind and temperature fields as well as in the sea ice cover. We observe a strong significant increase in the frequency of Atlantic Ridge in the second year after equatorial eruptions that precede the NAO + detected in year 3–5 as a result of a strong zonal wind anomalies in year 1–2. Evidence for a stronger polar vortex is detected in years 12–14 where NAO + is detected both as a frequency increase and in the wind and temperature fields. A short-term response is also detected 2–4 years after NH eruptions. The longterm signal after NH eruptions indicate a weak polar vortex around a decade after an eruption. Although the signal after NH eruptions is weaker our results stress the need for further studies. The simulated atmospheric response recorded in ECHAM5 after volcanic eruptions suggest a more dynamic response than previously thought. The methodology used can also be applied to other forcing scenario, for example for future climate projections where the aim is to search for a long-term climate signal.

1. Introduction

Volcanic sulphate aerosols reaching the stratosphere after major eruptions are well known for their impact on global climate. Sulphate aerosols form when sulphur dioxide from an eruptive plume reacts with water. Due to their chemical properties the aerosols scatter short-wave radiation cooling the Earth's surface in the first 1–2 years after an eruption, while absorbing terrestrial long-wave radiation warming the stratosphere (Deirmendjian, 1973; Toon and Pollack, 1980). In addition the sulphate aerosols, as well as volcanic halogens, cause ozone depletion that leads to stratospheric cooling at the poles (Stenchikov et al., 2002). Although volcanic ash falls out due to gravity within few months it too absorbs terrestrial long-wave radiation causing a warm layer in the stratosphere. All of the above mentioned particles cause changes in both the horizontal and meridional atmospheric temperature gradient that can lead to changes in temperature and pressure patterns in the troposphere (Shindell et al., 2009). This mechanism has the potential to result in decadal influences of volcanic eruptions on the climate system of the Earth as a result of the dynamic interactions between the atmosphere and ocean.

Volcanic impact on climate was previously thought to be limited to 1–3 years (Robock, 2000; Stenchikov et al., 2002). However, more

* Corresponding author at: Institute of Earth Sciences, University of Iceland, Iceland.
E-mail address: hera@hi.is (H. Guðlaugsdóttir).

https://doi.org/10.1016/j.atmosres.2018.04.021
Received 3 January 2018; Received in revised form 20 April 2018; Accepted 24 April 2018
Available online 02 June 2018

recent studies have shown that radiative surface cooling due to strong volcanic eruptions in the first years after an eruption can initiate a dynamical climate response by influencing the Atlantic Meridional Overturning Circulation (AMOC), that can in turn delay the recovery of the climate system on a decadal to multi-decadal scale (Church et al., 2005; Gleckler et al., 2006; Stenchikov et al., 2009; Otterå et al., 2010; Zanchettin et al., 2012). Swingedouw et al. (2015) showed using both simulations and proxy records that moderate volcanic eruptions, similar to the Agung eruption in 1963, exhibit an important role in the 15–20 year cycle of the AMOC. The authors hypothesize that the triggering mechanism between the volcanic eruptions and the AMOC is due to an increase in sea ice cover in the Nordic Seas.

In the North Atlantic region (90°W-45°E / 30–90°N) the leading mode of the climate system is the North Atlantic Oscillation (NAO), defined as the first Empirical Orthogonal Function (EOF) of sea level pressure over the Atlantic sector in winter (Hurrell, 1995). This oscillating pressure system between the Icelandic Low and the Azores High controls the strength and direction of westerly winds blowing over the North Atlantic and Western Europe, affecting temperature and precipitation patterns in the North Atlantic (Hurrell, 1995). Although the NAO is partly controlled by the behaviour of the stratospheric polar vortex as a result of planetary wave formation and transportation (Perlwitz and Graf, 1995), sea surface temperature (SST) has also been shown to be a contributing factor (Gastineau and Frankignoul, 2015). The NAO has two phases, the positive (NAO+) and the negative (NAO−) phase. NAO+ is identified by stronger westerlies resulting in warmer temperatures and more precipitation over Northern Europe and East USA while the opposite is true for the NAO−.

Winter atmospheric variability has been investigated by Cassou et al. (2004) where they identified four weather regimes over the North Atlantic-European region, namely the NAO+, NAO−, a strong anti cyclonic ridge known as the Atlantic Ridge (AtR), also known as the East Atlantic Pattern, and a pressure dipole between Scandinavia and Greenland known as the Scandinavian Blocking (ScB). ScB is a persistent anticyclone blocking circulation that results in stagnant climate in the area of its geographic location. Ortega et al. (2014) observed that these four weather regimes leave a clear imprint in isotope records from Greenland ice cores and are an important part of the climate system over the North Atlantic. As opposed to NAO+, the NAO− and both ridges and blocking patterns can be linked to a weaker Polar Vortex.

The role of volcanism in the phasing of NAO has been the focus of many studies. Results have shown that large equatorial volcanic eruptions tend to force the winter NAO into a positive phase in the first few years after an eruption. That is a result of planetary wave amplification due to an increase in the equator-to-pole temperature gradient that in turn strengthens the Polar Vortex (PV), causing a warming in Northern Europe (Robock and Mao, 1992; Graf et al., 1994; Kodera, 1994; Fischer et al., 2007). This was also observed in the millennial NAO reconstructions by Ortega et al. (2015) where an increase in NAO+ emerged two years after strong volcanic eruptions. Zanchettin et al. (2013) showed by analyzing the signature of strong tropical volcanic eruptions in eight runs of ECHAM5-MPI/OM that an increase in the winter (December–January- February - DJF) NAO+ signal accompanied by an increase in European SST suggests a warm climate event peaking about a decade after an eruption.

Most of these earlier studies investigating the North Atlantic climate response to volcanic forcing were focused on equatorial large volcanic eruptions, associated with poleward spreading, and thus longer lifetime, of volcanic aerosols. The impacts of high latitude Northern Hemisphere (NH) eruptions on atmospheric dynamics remain to be investigated to a similar extent. High latitude winter eruptions, occurring during local insolation minimum, are known to have local radiative impact (Oman et al., 2005) but only little global climate impacts (Kravitz and Robock, 2011). In climate simulations, equatorial eruptions and high latitude summer eruptions tend to impact most strongly the Arctic region during winter months, involving responses in the atmospheric and ocean circulation as well as amplifying Arctic sea ice feedbacks Schneider et al. (2009). Pausata et al. (2015) concluded that high latitude eruptions leave a long lasting impact in the climate system by influencing the ocean heat content and therefore the AMOC that in turn influences the El Niño Southern Oscillation (ENSO). However, it is still an unresolved question what the sensitivity of the climate system is to volcanic eruptions.

In this study, we analyze the volcanic fingerprint in the North Atlantic atmospheric circulation winter dynamics through the simulated response of the four dominant regional weather regimes (NAO+, NAO−, ScB, AtR) as well as the temperature at 2 m (*T2m*) and 250mb zonal wind (*u-wind*) fields and sea ice cover response. For this purpose, we use the output from six fully coupled ECHAM5/MPI-OM ensemble runs. This includes separate analyses of the response to equatorial and NH (high latitude) eruptions.

2. Methods

To carry out this study we use the 500mb geopotential height output from six ensemble runs spanning 800–2000 CE. Five are from an ECHAM5/MPI-OM fully coupled atmosphere-ocean model of the Millennium Community Earth System Model (COSMOS) experiment (ECHAM5-mil) described in Jungclaus et al. (2010). These five ensemble members are referred to as mil 10, mil 12, mil 13, mil 14 and mil 15 (no mil 11). The sixth member (ECHAM5-main) is the most recent run carried out in 2014 also using the ECHAM5/MPI-OM, but run with an updated solar forcing, prescribed vegetation and CO_2 (Sjolte et al., 2018). In all cases the boundary conditions and forcings for the model runs are the same except for slight changes in the ocean initial conditions. The atmospheric component ECHAM5 is run in T31 resolution corresponding to 3.75° × 3.75° and 19 vertical levels up to 10 hPa. Thus it is a low top model that does not include the important variability of the upper stratosphere, i.e. the Quasi Biennial Oscillation, and as such has its limitations. The forcing of this transient model run includes greenhouse gases, volcanic aerosols, total solar irradiance, vegetation changes and land-use and orbital forcing (Table T1), similar to the Last Millennium simulations performed within the Coupled Model Inter-comparison Project CMIP5 (Schmidt et al., 2011). According to Crowley et al. (2008) volcanic forcing is specified as aerosol optical depth (AOD) and effective radius (Reff) for 30–90 and 0–30 latitudinal bands on each hemisphere. The AOD is a measure of stratospheric transparency to incoming solar radiation. Past AOD reconstructions are based on a calibration of polar ice core sulphate records against satellite AOD (Crowley et al., 2008). The Total Solar Insolation (TSI) forcing used in our simulation is similar to the Krivova reconstruction used by Jungclaus et al. (2010) but with slightly larger variability and a reduced modern maximum (Text S1) to better match reconstructions from the new sunspot calibration (Krivova et al., 2007).

To identify the four main weather regimes in the NA for the period 800–2000 CE in each of the six runs we followed the same approach as Ortega et al. (2014) where K-means clustering (Hartigan, 1975) was applied, to each run, on the monthly mean standardized matrix of winter months (DJF) 500 mbar geopotential height (gph). The mean value of 200 K-means clustering repetitions represents the most stable clusters (Cassou et al., 2005) for the winter months of the 1200-year period where the number of centroids is set to be 4 (k = 4) according to Ortega et al. (2014) and references therein. The clustering method also assigns indices (1–4) to each month, depending on which centroid the DJF 500 mbar gph belongs to under the conditions of minimizing the squared Euclidean distance between the different centroids and their assigned 500 mbar gph patterns. This allows for the calculation of the frequency of each regime for a given time interval. For each run, indices of the full 1200-year period result in a mean frequency signal serving as an analogue of the mean North Atlantic climate state as displayed in the weather regimes. In this study we are interested in detecting both inter-decadal and decadal climate anomalies of volcanic origin. Therefore we

Table 1
Selected equatorial and NH volcanic eruptions for analysis of weather regime response.

Eruption	Eruption year	ECHAM5 forcing start	Year 0	Year of max. forcing	Max AOD	Max Reff
Equatorial						
Unknown	854	854.01	854	854.08	0.22	0.60
Unknown	1228	1228.01	1228	1229.02	0.38	0.73
Samalas	1257	1257.09	1258	1258.05	0.70	0.89
Huyaputina	1600	1600.01	1600	1600.09	0.35	0.70
Parker	1640	1640.12	1641	1641.08	0.33	0.69
Gamokara	1673	1673.05	1673	1673.12	0.22	0.60
Banda Api	1694	1694.03	1694	1694.11	0.24	0.62
Tambora	1815	1815.04	1815	1815.12	0.47	0.78
Cosiguina	1835	1835.01	1835	1835.09	0.24	0.62
Krakatau	1883	1883.08	1884	1884.04	0.23	0.61
Agung	1963	1963.11	1964	1964.07	0.16	0.54
NH						
Unknown	814	814.01	814	814.04	0.25	0.63
Vatnaöldur?	874	874.01	874	874.04	0.11	0.48
Eldgjá?	940[a]	940.04	940	940.08	0.16	0.54
Krísuvík?	1165	1165.07	1165	1165.10	0.14	0.51
Unknown	1585	1585.01	1585	1585.04	0.29	0.66
Laki	1783	1783.09	1783	1784.01	0.25	0.63

Equatorial volcanic eruptions are prescribed in all four latitude bands except for the eruption at 854 CE and 1641 CE that were prescribed in only three (30–90°N, 30–0°N and 0–30°S) latitudinal bands. NH volcanic eruptions are prescribed according to AOD > 0.1 and Reff > 0.4, with an effect only being present in the northern most latitude band (30–90°N). Year 0 is the year prior to the maximum forcing.

[a] The revised timescale by Sigl et al. (2009) assigns Eldgjá to the eruption year 940 CE.

apply the clustering method on 1200 years of winter months that in total are 3600 months for each run. We analyze a 50-year (147 months) running window in 5-year steps, i.e. the periods 800–849, 805–854. By doing so, the mean frequency of each 50-year period can be calculated where the 5-year step serves to capture climate anomalies within these 50-year periods. The total number of periods clustered in each run is 231. This results in a frequency signal serving as an analogue of high frequency North Atlantic climate state for the whole model run. The clustering method yields indices for each period clustered that are further used to detect a volcanic signal within each weather regime by selecting relevant volcanic winter months. This procedure is repeated for each run and the average used for further analysis.

The volcanic analysis is divided into 11 large equatorial eruptions and 6 high latitude eruptions (Table 1). Volcanic eruptions are selected according to the prescribed volcanic loading for the ECHAM5 simulation (Jungclaus et al., 2010; Crowley et al., 2008). Only eruptions that have limited or no interference with other eruptions are selected, explaining the difference in the numbers of selected eruptions for NH and low latitudes. This imbalance might influence our attempt to detect a climate signal after NH eruptions in ECHAM5. The volcanic forcing of the 11 selected equatorial eruptions is prescribed in all four latitude bands except for the eruptions at 854 CE and 1641 CE that were prescribed in only 30–90°N, 30–0°N and 0–30°S latitudinal bands, respectively. The eruptions of Santa Maria in 1902 and Novarupta in 1912 were left out due to the number of years between the two eruptions being < 20. Large volcanic loading in all bands is detected in 1456 (the Kuwae volcanic event was in 1452/1453) but the duration is unusually long and consists of multiple eruptions so it was excluded from our analysis. The 6 selected NH high latitude eruptions are based on eruptions with AOD > 0.1 and Reff > 0.4, with an effect only being present in the northern most latitude band (30–90°N). Year 0 (DJF of year 0) is defined as the year where the forcing has begun but the maximum forcing has not yet been reached. For some eruptions the forcing is not present in all three winter months in year 0, i.e. Eldgja where Dec is without forcing (Dec of 939, Jan 940 and Feb 940). Year 1 is defined as the first winter after the maximum forcing.

We assess the effect from individual volcanic eruptions by extracting winter month time series from 2 years prior to an eruption (for statistical reference) to 20 years after. The climate response to volcanic eruptions may extend into longer timescales, not explored here. The indices resulting from each of the moving clustered windows in the K-means clustering are selected to cover the years with volcanic eruptions used for the analysis. The equatorial analysis forms a 33 × 23 matrix (DJF of 11 eruptions, 23 years) and the NH analysis 18 × 23 matrix (DJF of 6 eruptions, 23 years) where the number of each indices results in a volcanic frequency series for each weather regime spanning 23 years. The volcanic frequency series are stacked according to Superposed Epoch Analysis (SEA) (Chree, 1912, 1913). This is repeated for each individual ensemble run and their mean signal used in estimating the volcanic impact. To analyze the sea ice response EOF analysis was performed and the first principal component (PC) time series was retrieved as for the weather regime analysis and stacked according to SEA, both for equatorial and NH eruption.

2.1. Estimating statistical significance

To estimate the statistical significance of the observed annual signal, we bootstrap the weather regime frequency series for calculation of the 95% confidence interval (c.i.) (Text S2). This estimation is done both for NH and equatorial volcanic eruptions. To test the significance of the volcanic frequency signal, error bars were calculated based on random occurrence of frequency of the individual weather regimes for DJF of 800–2000 CE, similar to the approach of Zanchettin et al. (2012). The total clustered period (1200 years) was used to select 11 winter years randomly a 1000 times from the indices and the mean and standard deviation used in the same way as for bootstrapped c.i, except here n is the number of ensemble members ($n = 6$). The peaks that go over/under the error bars show deviation from the climate baseline and are considered to be of volcanic origin. This was repeated for NH eruptions (6 winter years). Calculation of statistics to estimate sea ice cover is the same except the first PC from the EOF analysis is used.

To further estimate the significance of the modeled frequency signal and the climate impact after volcanic eruptions, as well as gaining a fuller insight into the performance of the model itself, the *T2m* anomaly fields as well as the *u-wind* anomaly fields at the 250mb level were analyzed for all significant years after both EQ and NH eruptions. Indices from the clustering of the 500mb gph (3600 winter months) were used to retrieve the associated *T2m* and *u-wind* average field pattern for each regime. This was again repeated for each model run and the average pattern calculated and used to identify the regimes that

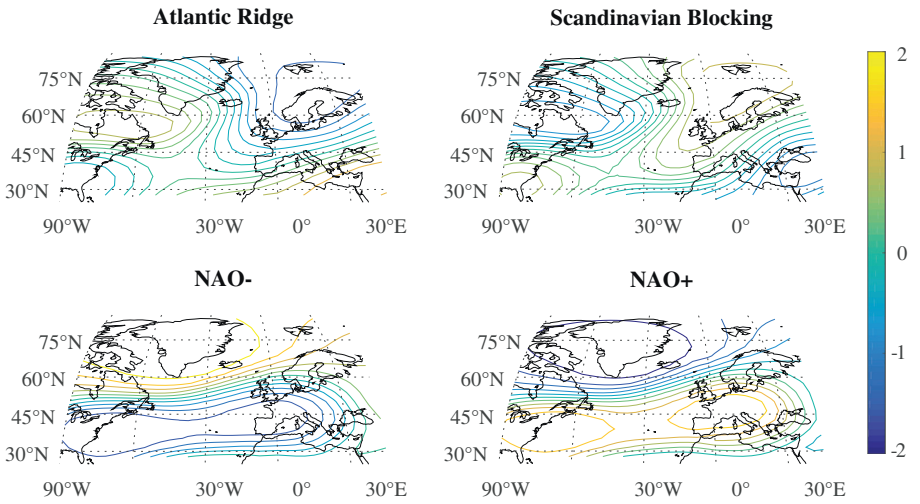

Fig. 1. The average winter North Atlantic weather regime patterns identified by the clustering method for the full period 800–2000 CE calculated for all six runs. Colour bars represent normalised (z-score) 500mb geo-potential height for each regime. The two upper panels show the pattern of AtR and ScB. AtR has centres of action over Scandinavia (negative pressure anomalies) and the Labrador Sea (positive pressure anomalies). ScB has anticyclone circulation located over Scandinavia (positive pressure anomalies) and cyclonic circulation over Newfoundland (negative pressure anomalies). The lower two panels are the well-known patterns of the positive and negative phase of the North Atlantic oscillation. The regimes are clearly identified in each run when clustering the full period, with an exception in mil0015 where location of centres of height in AtR and ScB are slightly different compared to the other runs (not shown). (For interpretation of the references to color in this figure legend, the reader is referred to the web version of this article.)

might be present. Both the *T2m* and *u-wind* anomalies for each significant post-volcanic year according to the clustering analysis were calculated with respect to 15 years prior to each event. That was done in order to remove the possible climatic trends, e.g. the little ice age, from the years analyzed. Usually the weather regimes can be identified visually but to strengthen such identification, both the correlation coefficients (r and p) and the Root Mean Squared error (*RMSe*) between the significant years and each of the weather regimes were calculated. The reason why r, p and *RMSe* are used lies in the symmetric nature between NAO− and NAO+ as well as ScB and AtR. Results are provided in supplementary Tables T2 and T3.

3. Results

3.1. Weather regimes in the North Atlantic: Climate baseline

The governing North Atlantic weather regimes (90 W-45E/30-90 N), AtR, ScB,

NAO− and NAO+, were identified in all six ECHAM5/MPI-OM coupled simulations by the K-means clustering method for the full period 800-2000 CE. Their average pattern is presented in Fig. 1. The resulting frequency of each weather regime during the full model period is presented in Fig. 2. The difference between ECHAM5-mil and ECHAM5-main is mainly observed for NAO− and NAO+, especially in 1600 CE and onwards, but otherwise the trends between runs are similar. The difference between ECHAM5-mil and ECHAM5-main is mainly observed for NAO− and NAO+, especially in 1600 CE and onwards, but otherwise the trend between runs is similar.

3.2. Volcanic analysis: Equatorial eruptions

The average stacked climatic response to equatorial eruptions (11 eruptions) calculated from all six ensemble-runs is shown in Fig. 3, left panel. The peaks that go over/under the error bars show deviation from the climate baseline and are thus considered to be of volcanic origin. For AtR, a strong significant (> 95% confidence level) increase in frequency in year 2 followed by an increase in the frequency of NAO+ in year 3–5, reaching a maximum is observed in year 4. Again, AtR shows a weak significant frequency increase in year 12 and NAO+ in year 13. No significant signal is observed for NAO−.

Since the significance level is 95%, it is expected that one year out of twenty becomes significant due to chance alone. In cases where two years or more are significant, sea ice was also considered for all ensemble runs where EOF analysis was performed and the 1st PC used. For equatorial eruptions a sharp significant increase in sea ice cover occurs in year 1 after an eruption that reaches a maximum in year 2, coinciding with the AtR increase in year 2 (left panel, Fig. 3). After that, sea ice gradually decreases until it reaches a normal state (within the green error bars) in year 10 and onwards.

3.3. Volcanic analysis: high latitude eruptions

The stacked climatic responses to high-latitude eruptions (6 eruptions) are shown in Fig. 3, right panel. Again, the peaks that go over/under the error bars show deviation from the climate baseline and are thus considered to be of volcanic origin. Nothing of significance is observed for AtR while a frequency decrease of ScB becomes weakly significant in year 12. A significant NAO− frequency increase occurs in year 15 and again in year 17 (weak increase). Then a weak significant frequency increase is detected in for NAO+ in year 2. The 1st PC of sea ice cover was also analyzed by method of SEA for NH eruptions. Compared to equatorial eruptions similarities are less clear between signal in the weather regimes and sea ice, where sea ice cover shows a significant decrease in year 3 and 10 after an NH eruption (bottom right panel, Fig. 3). However the signal observed in the sea ice cover in year 3 agrees with the signal detected in the NAO+ in year 2, although this relationship is weak.

3.4. T2m and u-wind analysis

To further investigate the results from the clustering analysis, composite *T2m* and *u-wind* fields were also analyzed where the *T2m* and *u-wind* pattern associated with each regime (Fig. F1) was retrieved as described in Methods. The composite fields of years 0–5 and 9–14 after EQ eruptions, both for *T2m* and *u-wind*, that were constructed in order to cover years of significance are shown in Figs. 4 and 5. According to Fig. 4, upper panels, negative *T2m* anomalies are present over most of the North Atlantic in years 0–3 where year 2 is assigned to NAO− according to Table T2 ($r = 0.63$). Positive *T2m* anomalies begin to emerge in year 4 and 5 where NAO+ is assigned to both years ($r = 0.57$ and $r = 0.72$ respectively). The *u-wind* (Fig. 4, lower panels) shows a strong increase in positive *u-wind* anomalies in year 1–2 where year 2 is assigned to NAO− ($r = 0.61$). In agreement with the *T2m* fields, years 4–5 are assigned to NAO+ ($r = 0.93$ and $r = 0.79$ respectively). In Fig. 5, upper panels, *T2m* fields in years 10–11 are assigned to AtR according to T2 ($r = 0.52$ and $r = 0.64$ respectively). However, the *u-wind* does not agree (Fig. 5, lower panels) where years 10–12 are assigned to NAO+ ($r = 0.55$, $r = 0.77$ and $r = 0.67$ respectively). A clear NAO+ signal emerges in year 14 detected in both *T2m* and *u-wind* ($r = 0.92$ and $r = 0.83$ respectively).

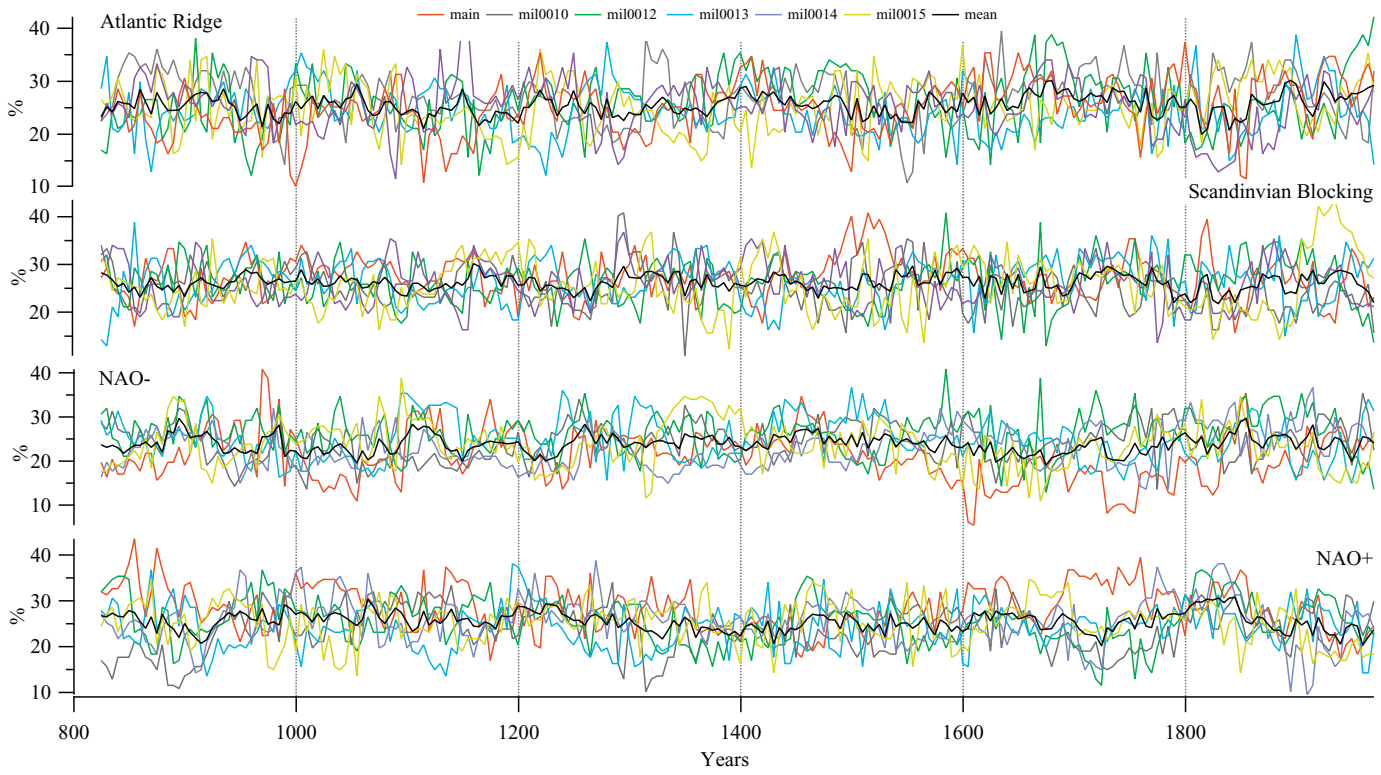

Fig. 2. Frequency variability of NAO+ and NAO−, ScB and AtR for all ensemble runs for the full model run. Black line is the ensemble-mean for each weather regime, red is main run, gray is run mil0010, green is run mil0012, blue is run mil0013, purple is run mil0014 and mustard is run mil0015. (For interpretation of the references to color in this figure legend, the reader is referred to the web version of this article.)

The NH years analyzed have a much weaker significant signal in the clustering analysis compared to the EQ eruptions, while a much clearer signal emerges in the field analysis as can be observed in Figs. 6–8. Positive *T2m* anomalies are present in years 0–4 over most of the North Atlantic after NH eruptions, where year 2 and 4.

($r = 0.59$ and $r = 0.58$) are assigned to NAO+, while year 3 is assigned to ScB ($r = 0.62$) according to Table T3. The *u-wind* field (Fig. 6, lower panels) agrees with *T2m* in year 2 where NAO+ is also detected

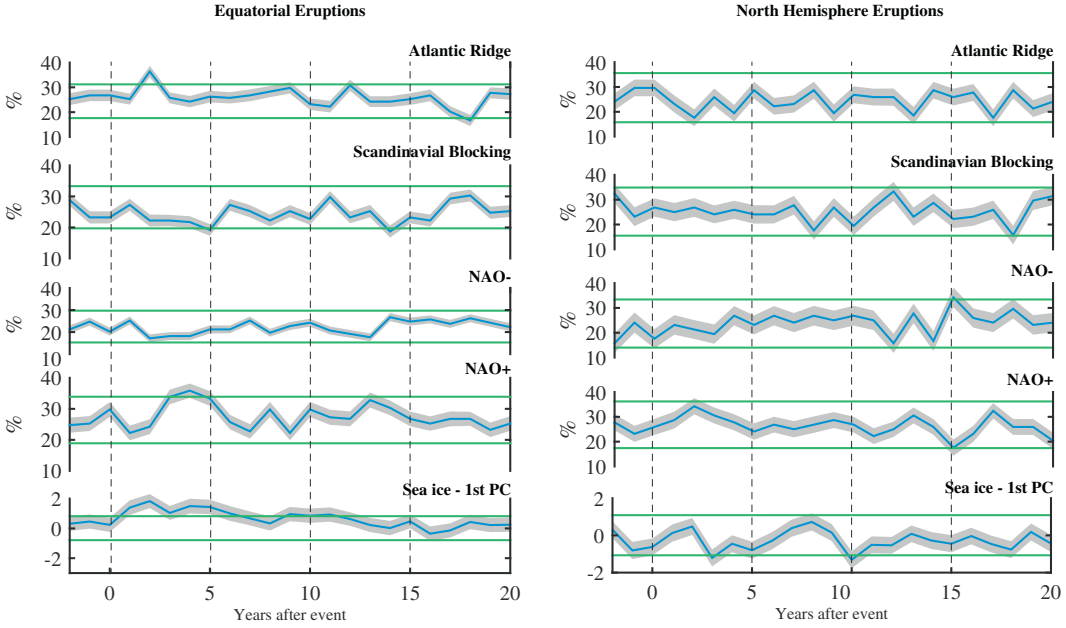

Fig. 3. Analysis of response to equatorial volcanic forcing in winter AtR, ScB, NAO−, NAO+ and 1st PC of sea ice cover 2 years prior to an eruption (year 0) to 20 years after by methods of stacking (SEA). Left panels: Equatorial volcanic analysis, Right panels: North Hemisphere volcanic analysis. Green lines are (95%) error bars and the area between the upper and lower lines defines the mean climate based on the ensemble-mean. The blue line is the ensemble-mean of the stacked response and grey shadings are 95% confidence interval calculated from bootstrapping. (For interpretation of the references to color in this figure legend, the reader is referred to the web version of this article.)

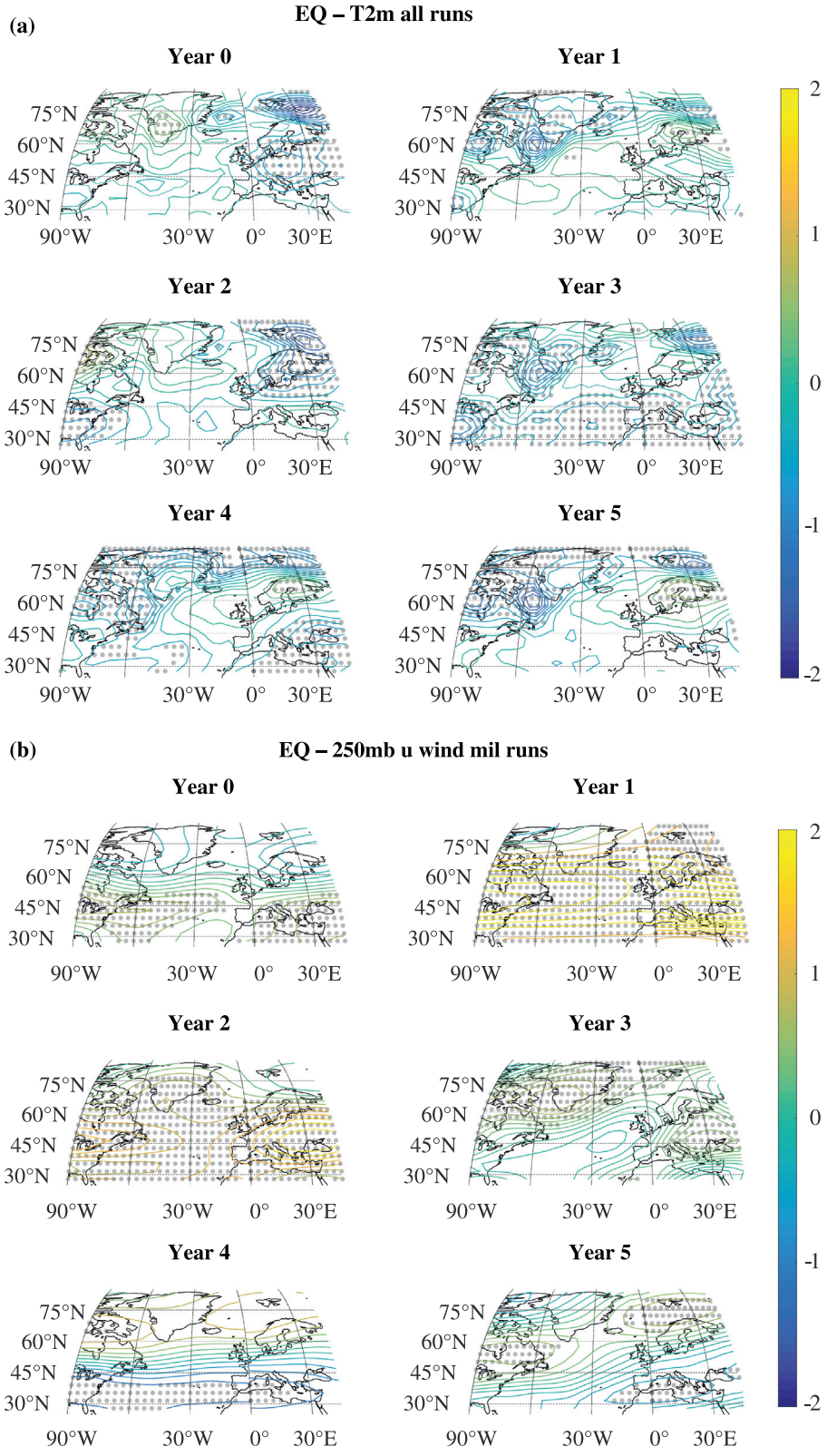

Fig. 4. Composite *T2m* and *u-wind* field anomalies 0–5 years after EQ eruptions. Anomalies are calculated with respect to 15 years prior to each eruption. Dotted areas are significant in the 95% interval according to a Student's *t*-test where anomalies are calculated according to 15 years prior to each event.

(r = 0.65). In Fig. 7, years 10–12 are assigned to NAO− (r = 0.75, r = 0.42, r = 0.83 respectively) where the *u-wind* agrees with the *T2m* in year 10–11 (r = 0.74 and r = 0.47). Year 13 is assigned to NAO+ in both *T2m* and *u-wind* (r = 0.58 and r = 0.80 respectively) while year 14 is assigned to NAO− (T2m: r = 0.51, u-wind: r = 0.30). The signal present in year 14–18 after NH eruptions is weak, where clustering analysis and field analysis are in little agreement.

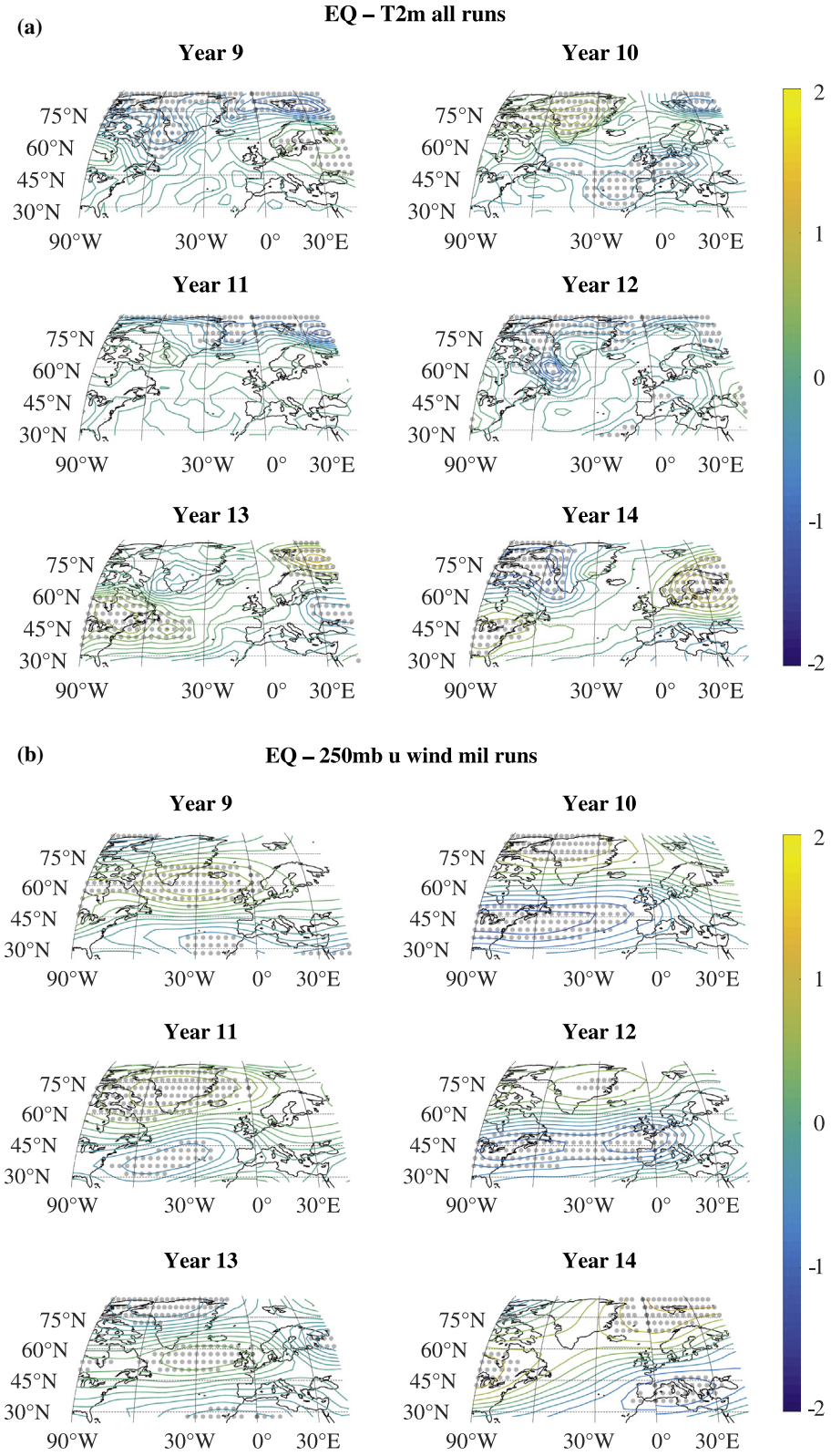

Fig. 5. Composite *T2m* and *u-wind* field anomalies 9–14 years after EQ eruptions. Anomalies are calculated with respect to 15 years prior to each eruption. Dotted areas are significant in the 95% interval according to a Student's *t*-test where anomalies are calculated according to 15 years prior to each event.

4. Clustering vs. field analysis

4.1. Equatorial eruptions

According to the *T2m* and *u-wind* field analysis (FA) the clustering analysis (CA) method captures most of the atmospheric circulation response after volcanic eruptions. The significant increase in the 250mb *u-wind* anomaly field, indicating a strengthened Polar Vortex, over most of the North Atlantic area in year 1–2 after EQ eruptions (Fig. 4) does not result in a clear weather regime patterns in the *T2m* field of year

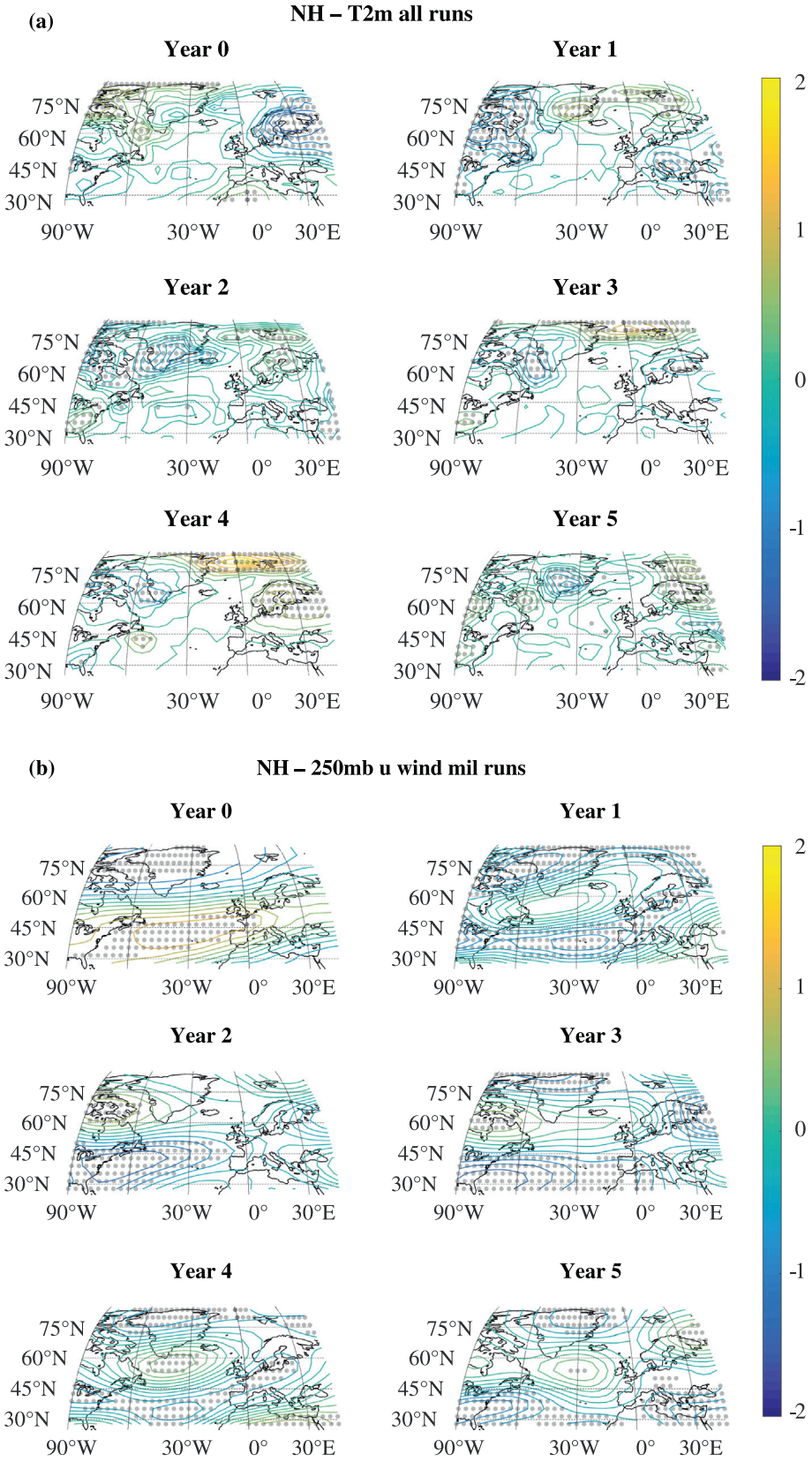

Fig. 6. Composite *T2m* and *u-wind* field anomalies 0–5 years after NH eruptions. Anomalies are calculated with respect to 15 years prior to each eruption. Dotted areas are significant in the 95% interval according to a Student's *t*-test where anomalies are calculated according to 15 years prior to each event.

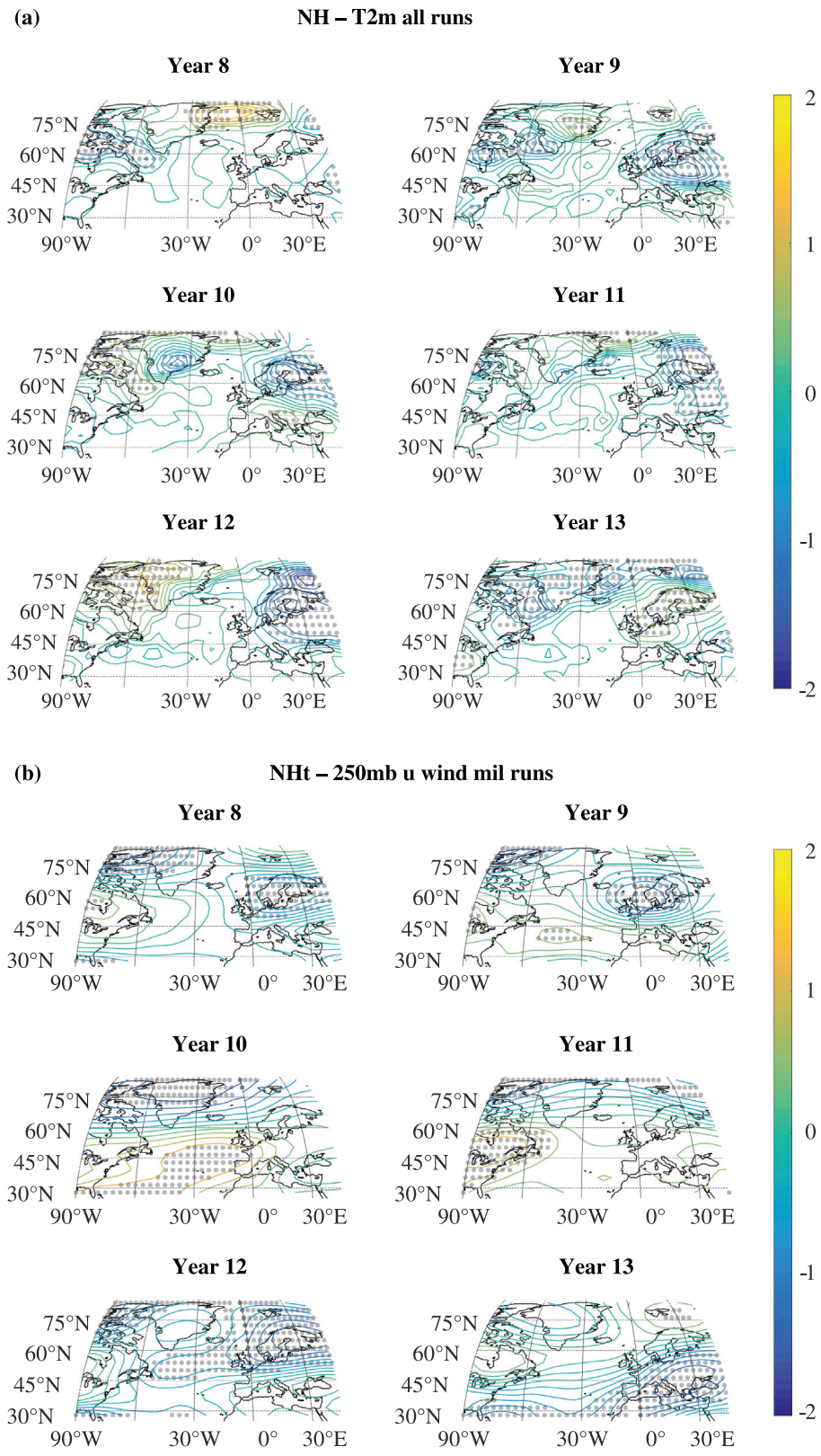

Fig. 7. Composite *T2m* and *u-wind* field anomalies 8–13 years after NH eruptions. Anomalies are calculated with respect to 15 years prior to each eruption. Dotted areas are significant in the 95% interval according to a Student's *t*-test where anomalies are calculated according to 15 years prior to each event.

1–2, where no evidence of NAO+ is present. Also, the AtR signal in year 2 in the CA is not clearly detected in the FA. While the RMSe (Table T2) is lowest between years 2–3 and AtR, the CorrCoef does not agree where it assigns NAO− to year 2 and NAO+ to year 3 (low CorrCoef for *T2m*). Thus a clear atmospheric circulation response is not detected in the first 1–3 years after EQ eruptions. Keeping in mind the nature of the clustering method (see Methods) and the average cluster fields in Fig. 1, the strong AtR frequency signal in year 2 could be a

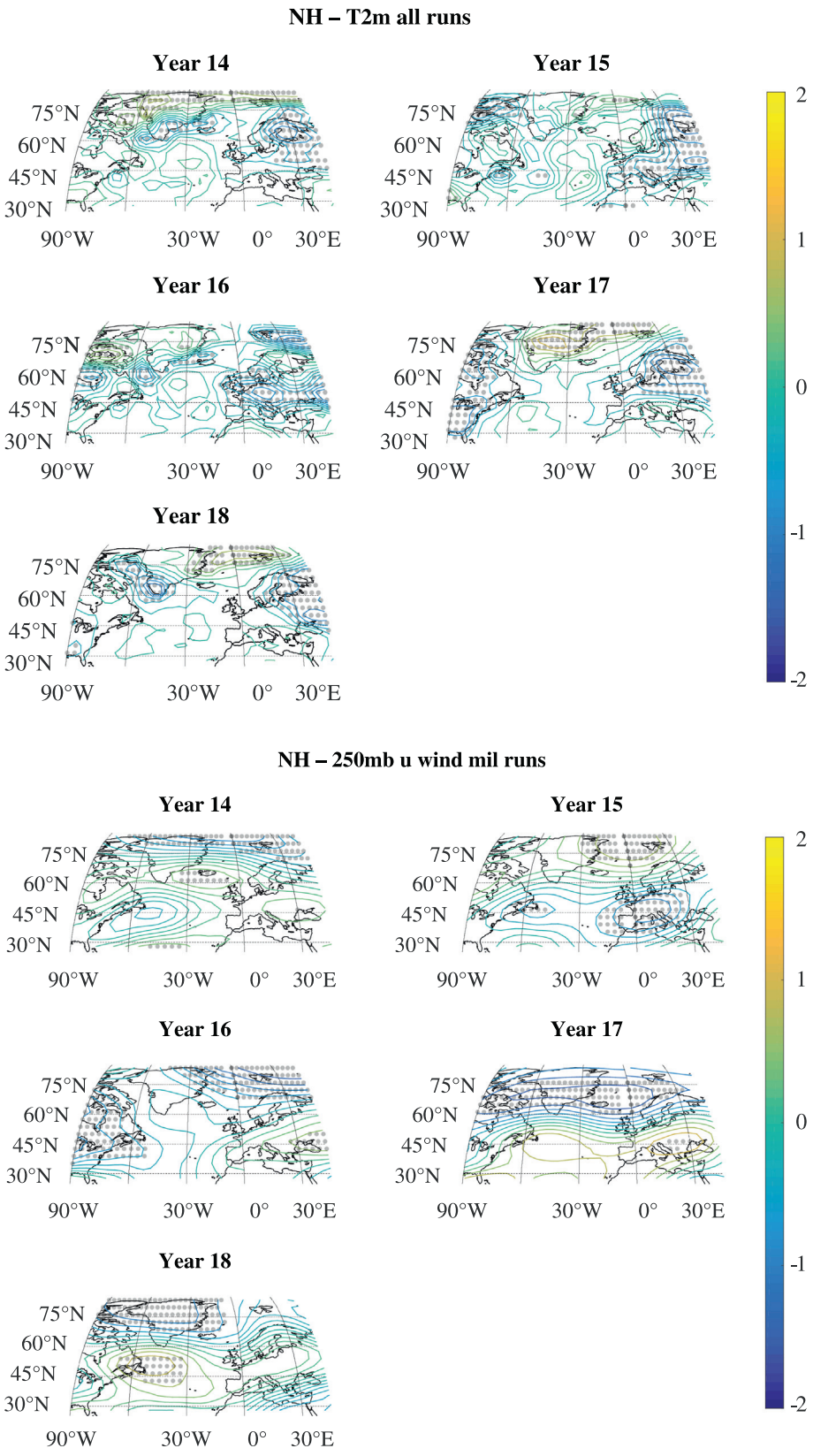

Fig. 8. Composite *T2m* and *u-wind* field anomalies 14–18 years after NH eruptions. Anomalies are calculated with respect to 15 years prior to each eruption. Dotted areas are significant in the 95% interval according to a Student's *t*-test where anomalies are calculated according to 15 years prior to each event.

mixture of both AtR and NAO−. However since it is significant at the 95% level, it supports a signal of volcanic origin. According to years 4–5, an NAO+ pattern emerges in the *T2m* and *u-wind* fields according to a CorrCoef $r = 0.57$ (*T2m*) and $r = 0.93$ (*u-wind*) for year 4 and $r = 0.72$ (*T2m*) and $r = 0.79$ (*u-wind*) for year 5, agreeing with the NAO + frequency increase in 3–5 in the CA. The *T2m* response show negative anomalies over most of the North Atlantic in years 0–5, agreeing with the sea ice analysis. In years 12 and 14 (Fig. 5) a clear NAO+ pattern, especially for year 14, occurs in the *T2m* and *u-wind* fields that is consistent with a CorrCoef $r = 0.92$ and $r = 0.83$ for *T2m* and *u-wind* respectively. In the CA, a slight significant NAO+ increase is detected in year 12 that, along with FA, indicates a stronger Polar Vortex 12–14 years after equatorial eruptions.

4.2. North hemisphere eruptions

The response in the CA after NH eruptions is much weaker compared with the response after EQ eruptions. However, the *T2m* and *u-wind* anomalies both result in a NAO+ − like signal in year 2 according to T3 as well as the CA where a weak increase in the frequency of NAO + is detected in year 2. A warming in the *T2m* field is present in the Nordic Sea in year 3–4 (Fig. 6), similar to the EQ response. Furthermore, we see a significant decrease of sea ice in year 3 that is consistent with the detected warming in the Nordic sea according to the *T2m* field. However, the results of the FA are not clearly linked to the long-term atmospheric response. Although NAO− is present in the fields in years 10 and 14 (Figs. 7 and 8) and in the CA in year 15 (Fig. 3), further studies are needed to confirm a link between these observations. Sea ice cover decrease in year 10 agrees with the *T2m* fields in years 8–11 where a warming in the Nordic sea is detected in year 8, 9 and 11 and Baffin bay in year 10. None of the parameters studied agrees on the signal present in year 14–18 after NH eruptions.

The CA captures most of the short and long-term atmospheric circulation response although the nature of the clustering method might result in a false and/or mixed signal compared to the strong AtR frequency increase in year 2 for EQ eruptions. Although the response detected in the CA after NH eruptions is weaker compared to EQ eruptions, the signal that is present agrees well with that detected in the FA, both the short and long-term atmospheric circulation response.

5. Discussion

We detect a significant increase in AtR frequency in year 2 in the CA (Fig. 3, left panel). This pattern is not commonly associated as a response in circulation to EQ volcanic eruptions, and we investigate this further in the FA. Negative *T2m* anomalies are present in years 1–3 (Fig. 4), where year 2 shows strong similarities to NAO− (Table T2). Considering the 1200-year average *T2m* fields associated with AtR and NAO− (Fig. F1), they both show negative anomalies over the Nordic Sea. That, along with the surface cooling detected in *T2m* in years 1–3, indicates that AtR and NAO− detected in year 2 in both CA and FA respectively emerge as a result of this surface cooling. However, since the FA does not agree with the CA despite the strong AtR frequency increase in year 2, the case of a false and/or mixed signal cannot be ruled out. We do detect a clear and robust NAO+ signal in years 3–5 in both the CA (Fig. 3, left panel) and FA (Fig. 4) as a result of a Polar Vortex strengthening in the first 2 years after EQ eruptions. According to previous studies NAO+ would be expected in year 1–2 but surface conditions are not able to lead to NAO+, since NAO+ is related to winter warming (Graf et al., 1994; Robock and Mao, 1992; Kodera, 1994). In other words we present evidences where surface cooling, emerging as AtR and NAO− in year 2 in CA and FA respectively, dominates the atmospheric circulation response to EQ eruptions in the first 1–2 years after volcanic eruptions in ECHAM5. This indicates that the surface cooling as a result of EQ volcanic eruptions could be overestimated in ECHAM5, as it was shown for the CMIP5 model ensemble in Driscoll et al. (2012). After the direct aerosol effect has decreased 1–3 years after EQ eruptions, a robust NAO+ is detected in years 3–5 in both CA and FA that suggests dynamic ocean-atmosphere coupling (Cayan, 1992; Delworth and Zeng, 2016).

Strong significant increase in sea ice cover is detected for EQ eruptions reaching a maximum in year 2 and lasting well into the 10th year after an eruption (Fig. 3, left panel). This sea ice cover increase is possibly also linked to radiative cooling during summer, which is beyond the scope of this paper. Both the NAO+ and sea ice cover increase is in agreement with Zanchettin et al. (2012) where the same model (MPI-ESM) is used but a different statistical approach is applied to detect the impact of volcanic forcing. In their study they detected anomalous heat fluxes in the Barents Sea around a decade after volcanic eruptions due to strong AMOC-driven northward oceanic heat transport and NAO− related modifications of the sub polar gyre structure that is referred to as delayed winter warming. As would be expected this is in agreement with our results, although we detect a signal in years 12–14 but Zanchettin et al. (2012) 2 years earlier. This difference can be assigned to the different methodologies used. A weak NAO+ frequency increase is observed in year 13 (Fig. 3, left panel), and NAO+ pattern in both the *T2m* and *u-wind* is present in years 12 and 14 (Fig. 4). This atmospheric circulation response occurs as soon as the sea ice cover has reached a pre-volcanic state (curve within the green error bars) in year 13–14 (Fig. 3). Also, in a study by Mahajan et al. (2011), the AMOC index and Arctic sea-ice extent were found to be anti-correlated ($r = -0.4$). Although we are not directly analyzing the AMOC circulation, this anti correlation offers a link between the sea ice cover decrease detected in year 13–14 and the following NAO+ in years 12 and 14 in both CA and FA (Figs. 3 and 55 respectively) that would agree with the strong AMOC-driven northward oceanic heat transport detected in Zanchettin et al. (2012).

A significant frequency signal is detected in all weather regimes except AtR after NH eruptions (Fig. 3, right panel). However the CA signal is weak compared to the signal after equatorial eruptions, possibly because selected NH eruptions are too few in order to isolate a clear climate signal from the climatological noise. We propose that the expected mechanism after NH eruptions is a weakening of the Polar Vortex in the first 1–2 years after NH eruptions due to warming in the stratospheric high latitudes, thereby decreasing the equator-to-pole gradient. Our results show a decrease in sea ice cover in year 3 (Fig. 3, right panel), after NH eruptions. This coincides with a weak frequency increase in NAO+ in year 2 that is also consistent with a NAO+ pattern in the *T2m* and *u-wind* in year 2 (*T2m*: $r = 0.59$, *u-wind*: $r = 0.65$) coinciding with a clear warming in the Nordic seas in year 1–4 (Fig. 6). This is counter intuitive to what we expect since an increase in sea ice is linked to NAO+ as seen after EQ eruptions. A decrease in Arctic sea ice cover has been linked to a weakened Polar Vortex (Kim et al., 2014), thereby favoring blocking events that give rise to meridional winds and occasional northward heat transport. This we do observe in year 10 where the sea ice cover is significantly lower while NAO− is present in both the *T2m* and *u-wind*, showing a warming over West Greenland and the Baffin Bay area (Fig. 7). However, the CA does not detect anything in year 10 although a weak ScB increase and NAO− decrease is observed in year 12. In Year 17 an NAO− pattern emerges in the FA (Fig. 8), compared with year 15 in the CA (Fig. 3, right panel), in both the *T2m* and *u-wind* fields that coincide with a slight increase in sea ice in year 17. A decrease in sea ice, especially east off Greenland (Magnusdottir et al., 2004), is known to cause NAO− response possibly explaining the delayed NAO− frequency increase in year 15 but the causality for such a long-term response after NH eruptions is vague and a more detailed model evaluation regarding this mechanism would be needed. The clear surface temperature response in the first 2–4 years (Fig. 6) does indicate that the ocean heat transport is responsible for such long-term memory as for the EQ eruptions but more detailed model and in situ studies are needed to confirm such.

Since planetary wave formation depends i.e. on meridional

temperature gradient, equatorial eruptions tend to influence their formation more strongly compared to NH eruptions, as our results also suggests. Although NH eruptions are more dependent on the season of the eruption, they can in theory influence the meridional temperature gradient in the stratosphere. This should result in a weakened Polar Vortex in the first 1–2 years, as we propose, but our results are not clear since the sea ice cover decrease seen in our analysis is in support of such a weakening (Fig. 3, right panel), but the anomalies we see in *T2m* and *u-wind* are not (Fig. 6). Our results indicate that NH eruptions are not only recorded in the short-term memory of the climate system, but the long-term memory as well through the *T2m* anomaly response that is transported via North Atlantic gyre circulation. Furthermore, our results suggest an opposite decadal response after high and low latitude eruptions where NAO + emerges 12–14 years after EQ eruptions and NAO − emerges 10 years after NH eruptions. The mechanism behind such a long-term response after both EQ and NH volcanic eruptions is considered to lie within the AMOC (Slawinska and Robock, 2018; Pausata et al., 2015). Frankignoul et al. (2013) investigated different AMOC regimes and their effect on the atmospheric circulation variability. There they found that during AMOC intensification the regime referred to as the red-noise regime (strong multi-decadal variability) of the AMOC causes a northward shift of the Gulf Stream/North Atlantic Current and tends to lead to a positive NAO during winter. The oscillatory regime however (regular and strong decadal variability) causes a southward shift of the Gulf Stream/North Atlantic Current during AMOC intensification that results in an upper-ocean heat content anomaly proceeded by a negative NAO. Such a mechanism might be responsible, where EQ eruptions impact the red noise regime of the AMOC leading to the known northward ocean heat transport and NAO + while NH eruptions impact the oscillatory regime of the AMOC causing a southward shift in ocean heat transport and therefore NAO −. This stresses the importance of the meridional heat transport in the decadal response to both NH and EQ eruptions as well as the need for investigating this mechanism in detail in future studies, e.g. by the approach of Yang et al. (2015). Given that the version of ECHAM5 is a low-top model (lower stratosphere, 10 hPa) and thus does not capture fully the stratospheric dynamics, it will likely influence our results by dampening the observed signal.

6. Conclusions

Our investigations of the response of simulated 500mb gph weather regimes in the North Atlantic by the use of K-means clustering method, the sea ice cover response and *T2m* and *u-wind* field anomaly analysis to volcanic forcing are complementary to each other, where both equatorial and NH volcanic response has been identified in all four weather regimes. We present evidence where surface cooling dominates the atmospheric circulation, emerging as AtR and NAO −, in the first 1–2 years after EQ eruptions. However, due to the nature of the clustering method, the AtR signal might also be a mixture of both AtR and NAO − and therefore further studies are needed to explain this possible mechanism. In year 3–5 a robust NAO + signal emerges as a result of ocean-atmosphere coupling. We hypothesize that the decadal response in years 12–14 is mainly due to AMOC strengthening and northward oceanic heat transport as a result of the slow decadal sea ice decrease that reaches a pre-volcanic state in years 13–14, where AMOC releases thermal energy from the ocean up into the atmosphere resulting in an NAO + response.

NH high latitude eruptions do leave a weaker but significant short-term regional atmospheric circulation response in the first years after an eruption. This result is consistently seen in the clustering and both the *T2m* and *u-wind* field analysis as well as sea ice cover. A weakening of the Polar Vortex is not clearly detected in the first 1–2 years after NH eruptions, although expected due to the warming in the stratospheric high latitudes. In our analysis we do not see clear evidence of a significant long-term dynamic regional climate signal after NH eruption, but the signal that is present, i.e. in year 10, show evidences of a Polar Vortex weakening due to of southward oceanic heat transport. This emphasizes the need for a detailed study of the impact of NH eruption on the regional climate system.

Ocean circulation transporting thermal anomalies provides a key explanation in the observed memory in the climate system after both equatorial and NH eruptions. The response in the first 1–3 years after equatorial eruptions demonstrates a clear link between temperature, sea ice cover and atmospheric response in the North Atlantic region whereas we show evidence that the decadal response is more dominated by AMOC intensification due to sea ice cover decrease. Although the decadal response after EQ eruptions is much stronger, the NAO − signal present in the FA and the sea ice cover decrease in year 10 after NH eruptions indicates that the AMOC plays a role as well. However, further investigations are needed to understand the mechanisms of different atmospheric circulation responses to EQ and NH eruptions. Our CA methodology has proven to be efficient to capture both low and high frequency atmospheric circulation variability. Furthermore, it can be useful in analyzing long time series and/or model outputs where the aim is to probe for long-term climate signal on a decadal to centennial scale. It can also be applied to climate projections in order to decipher respective influences of volcanic as well as anthropogenic forcing on the regional atmospheric circulation, especially regarding the sensitivity of the Arctic region during its potential future warming.

Acknowledgements

We thank Raimund Muscheler for providing an updated reconstruction of total solar irradiance. We also thank the Alfred Wegener Institute (AWI) for accessing its high-performance computing systems to conduct the ECHAM5/MPI-OM simulation. Guðlaugsdóttir was supported by the Nordic Volcanological Centre (NordVulk) during this work. The output for the five COSMOS-MIL experiment runs Jungclaus (2008) can be obtained at the World Data Centre for Climate in Hamburg by request. Results from ECHAM5-main output analysis can be requested by contacting the author.

Appendix A. Supplementary data

Supplementary data to this article can be found online at https://doi.org/10.1016/j.atmosres.2018.04.021.

References

Cassou, C., Terray, L., Hurrell, J.W., Deser, C., 2004. North atlantic winter climate. regimes: Spatial asymmetry, stationarity with time, and oceanic forcing. J. Clim. 17 (5), 1055–1068.
Cassou, C., Terray, L., Phillips, A.S., 2005. Tropical Atlantic influence on european. heat waves. J. Clim. 18 (15), 2805–2811.
Cayan, D.R., 1992. Latent and sensible heat flux anomalies over the northern oceans: driving the sea surface temperature. J. Phys. Oceanogr. 22 (8), 859–881.
Chree, C., 1912. Some phenomena of sunspots and of terrestrial magnetism, at kew observatory. Philos. Trans. R. Soc. Lond. Ser. A (212), 75.
Chree, C., 1913. Some phenomena of sunspots and of terrestrial magnetism, ii. Philos. Trans. R. Soc. Lond. Ser. A (213), 245.
Church, J.A., White, N.J., Arblaster, J.M., 2005. Significant decadal-scale impact. of volcanic eruptions on sea level and ocean heat content. Nature 438 (7064), 74–77.
Crowley, T.J., Zielinski, G., Vinther, B., Udisti, R., Kreutz, K., Cole-Dai, J., Castellano, E., 2008. Volcanism and the little ice age. PAGES News 16 (2), 22–23.
Deirmendjian, D., 1973. On volcanic and other particulate turbidlty anomalies. Adv. Geophys. 16, 267–296.
Delworth, T.L., Zeng, F., 2016. The impact of the north atlantic oscillation on climate through its influence on the atlantic meridional overturning circulation. J. Clim. 29 (3), 941–962.
Driscoll, S., Bozzo, A., Gray, L. J., Robock, A., Stenchikov, G., 2012. Coupled Model Intercomparison Project 5 (CMIP5) simulations of climate following volcanic eruptions. J. Geophys. Res.: Atmospheres, 117 (D17).
Fischer, H., Siggaard-Andersen, M.L., Ruth, U., Röthlisberger, R., Wolff, E., 2007. Glacial/interglacial changes in mineral dust and sea-salt records in polar ice cores: Sources, transport, and deposition. Rev. Geophys. (1), 45.
Frankignoul, C., Gastineau, G., Kwon, Y.O., 2013. The influence of the AMOC variability on the atmosphere in CCSM3. J. Clim. 26 (24), 9770–9790.

Gastineau, G., Frankignoul, C., 2015. Influence of the north Atlantic SST variability on the atmospheric circulation during the twentieth century. J. Clim. 28 (4), 1396–1416.
Gleckler, P.J., AchutaRao, K., Gregory, J.M., Santer, B.D., Taylor, K.E., Wigley, T.M.L., 2006. Krakatoa lives: The effect of volcanic eruptions on ocean heat content and thermal expansion. Geophys. Res. Lett. (17), 33.
Graf, H.F., Perlwitz, J., Kirchner, I., 1994. Northern hemisphere tropospheric midlatitude circulation after violent volcanic eruptions. Contr. Atmos. Physics 67 (1), 3–13.
Hartigan, J.A., 1975. Clustering algorithms.
Hurrell, J.W., 1995. Decadal trends in the north atlantic oscillation: regional temperatures and precipitation. Science 269 (5224), 676–679.
Jungclaus, J., 2008. Mpi-m earth system modelling framework: millennium full forcing experiment. In: World Data Centre for Climate. CERA-DB.
Jungclaus, J.H., Lorenz, S.J., Timmreck, C., Reick, C.H., Brovkin, V., Six, K., Segschneider, J., Giorgetta, M.A., Crowley, T.J., Pongratz, J., Krivova, N.A., Vieira, L.E., Solanki, S.K., Klocke, D., Botzet, M., Esch, M., Gayler, V., Haak, H., Raddatz, T.J., Roeckner, E., Schnur, R., Widmann, H., Claussen, M., Stevens, B., Marotzke, J., 2010. Climate and carbon-cycle variability over the last millennium. Clim. Past 6, 723–737.
Kim, B.M., Son, S.W., Min, S.K., Jeong, J.H., Kim, S.J., Zhang, X., Shim, T., Yoon, J.H., 2014. Weakening of the stratospheric polar vortex by arctic sea-ice loss. Nat. Commun. 5, 4646.
Kodera, K., 1994. Influence of volcanic eruptions on the troposphere through stratospheric dynamical processes in the northern hemisphere winter. J. Geophys. Res.-Atmos. 99 (D1), 1273–1282.
Kravitz, B., Robock, A., 2011. Climate effects of high-latitude volcanic eruptions: Role of the time of year. J. Geophys. Res. 116 (D01105).
Krivova, N.A., Balmaceda, L., Solanki, S.K., 2007. Reconstruction of solar total. irradiance since 1700 from the surface magnetic flux. Astron. Astrophys. 467 (1), 246–335.
Magnusdottir, G., Deser, C., Saravanan, R., 2004. The effects of north atlantic SST and sea ice anomalies on the winter circulation in CCM3. part i: Main features and storm track characteristics of the response. J. Clim. 17 (5), 857–876.
Mahajan, S., Zhang, R., Delworth, T.L., 2011. Impact of the atlantic meridional overturning circulation (AMOC) on Arctic surface air temperature and sea ice variability. J. Clim. 24 (24), 6573–6581.
Oman, L., Robock, A., Stenchikov, G., Schmidt, G., Ruedy, R., 2005. Climatic response to high-latitude volcanic eruptions. J. Geophys. Res.-Atmos. (D13), 110.
Ortega, P., Swingedouw, D., Masson-Delmotte, V., Risi, C., Vinther, B., Yiou, P., Vautard, R., Yoshimura, K., 2014. Characterizing atmospheric circulation signals in. Greenland ice cores: insights from a weather regime approach. Clim. Dyn. 43 (9–10), 2585–2605.
Ortega, P., Lehner, F., Casado, M., Swingedouw, D., Masson-Delmotte, V., Yiou, P., Raible, C., 2015. A multi-proxy model-tested NAO reconstruction for the last millennium. Nature 57, 71–73.
Otterå, O.H., Bentsen, M., Drange, H., Suo, L., 2010. External forcing as a metronome for atlantic multidecadal variability. Nat. Geosci. 3 (10), 688–694.
Pausata, F.S.L., Chafik, L., Caballero, R., Battisti, D.S., 2015. Impacts of high latitude volcanic eruptions on ENSO and AMOC. Proc. Natl. Acad. Sci. U. S. A. 117 (45), 13784–13,788.
Perlwitz, J., Graf, H.F., 1995. The statistical connection between tropospheric and. stratospheric circulation of the Northern Hemisphere in winter. J. Clim. (10), 2281–2295.
Robock, A., 2000. Volcanic eruptions and climate. Rev. Geophys. 38 (2), 191–219.
Robock, A., Mao, J., 1992. Winter warming from large volcanic eruptions. Geophys. Res. Lett. 19 (24), 2405–2408.
Schmidt, G.A., Jungclaus, J.H., Ammann, C.M., Bard, E., Braconnot, P., Crowley, T.J., Delaygue, G., Joos, F., Krivova, N.A., Muscheler, R., Otto-Bliesner, B.L., Pongratz, J., Shindell, D.T., Solanki, S.K., Steinhilber, F., Vieira, L.E.A., 2011. Climate forcing reconstructions for use in PMIP simulations of the last millennium. (v1.0). Geosci. Model Dev. 4, 33–45.
Schneider, D.P., Ammann, C.M., Otto-Bliesner, B.L., Kaufman, D.S., 2009. Climate response to large, high-latitude and low-latitude volcanic eruptions in the Community Climate System Model. J. Geophys. Res.-Atmos. (D15), 114.
Shindell, D.T., Schmidt, G.A., Mann, M.E., Faluvegi, G., 2009. Dynamic winter. climate response to large tropical volcanic eruptions since 1600. J. Geophys. Res.-Atmos. (D5), 109.
Sigl, M., Winstrup, M., McConnell, J.R., Welten, K.C., Plunkett, G., Ludlow, F., Buntgen, U., Caffee, M., Chellman, N., Dahl-Jensen, D., Fischer, H., 2009. Timing and climate forcing of volcanic eruptions for the past 2500 years. Nature 523 (7562), 543–549.
Sjolte, J., Sturm, C., Adolphi, F., Vinther, B.M., Werner, M., Lohmann, G., Muscheler, R., 2018. Solar and volcanic forcing of north atlantic climate inferred from a processbased reconstruction. Clim. Past Discuss. http://dx.doi.org/10.5194/cp-2018-32. in review.
Slawinska, J., Robock, A., 2018. Impact of volcanic eruptions on decadal to centennial fluctuations of arctic sea ice extent during the last millennium and on initiation of the little ice age. J. Clim. 31 (6), 2145–2167.
Stenchikov, G., Robock, A., Ramaswamy, V., Schwarzkopf, M.D., Hamilton, K., Ramachandran, S., 2002. Arctic Oscillation response to the 1991 Mount Pinatubo. eruption: Effects of volcanic aerosols and ozone depletion. J. Geophys. Res.-Atmos. (D24), 107.
Stenchikov, G., Delworth, T.L., Ramaswamy, V., Stouffer, R.J., Wittenberg, A., Zeng, F., 2009. Volcanic signals in oceans. J. Geophys. Res.-Atmos. (D16), 114.
Swingedouw, D., Ortega, P., Mignot, J., Guilyardi, E., Masson-Delmotte, V., Butler, P.G., Khodri, M., Séférian, R., 2015. Bidecadal North Atlantic ocean circulation. variability controlled by timing of volcanic eruptions. Nat. Commun. 6, 6545.
Toon, O., Pollack, J., 1980. Atmospheric aerosols and climate: Small particles in the. Earth's atmosphere interact with visible and infrared light, altering the radiation balance and the climate. Am. Sci. 68 (3), 268–278.
Yang, H., Li, Q., Wang, K., Sun, Y., Sun, D., 2015. Decomposing the meridional heat transport in the climate system. Clim. Dyn. 44 (9–10), 2751–2768.
Zanchettin, D., Timmreck, C., Graf, H.F., Rubino, A., Lorenz, S., Lohmann, K., Jungclaus, J.H., 2012. Bi-decadal variability excited in the coupled ocean-atmosphere system by strong tropical volcanic eruptions. Clim. Dyn. 39 (1–2), 419–444.
Zanchettin, D., Timmreck, C., Bothe, O., Lorenz, S.J., Hegerl, G., Graf, H.F., Lutherbacher, J., Jungclaus, J.H., 2013. Delayed winter warming: A robust decadal response to strong tropical volcanic eruptions. Geophys. Res. Lett. 40 (1), 204–209.